Eigenvalue Optimization Algorithms for Structure/Controller Design Iterations

D.S. Bodden*
Virginia Polytechnic Institute and State University, Blacksburg, Virginia
and
J.L. Junkins†
Texas A&M University, College Station, Texas

An eigenspace optimization approach is proposed and demonstrated for the design of feedback controllers for the maneuvers/vibration arrests of flexible structures. The algorithm developed is shown to be equally useful in sequential or simultaneous design iterations that modify the structural parameters, sensor/actuator locations, and control feedback gains. The approach is demonstrated using a differential equation model for the "Draper/RPL configuration." This model corresponds to the hardware used for experimental verification of large flexible spacecraft maneuver controls. A number of sensor/actuator configurations are studied vis-a-vis the degree of controllability. Linear output feedback gains are determined using a novel optimization strategy. The feasibility of the approach is established, but more research and numerical studies are required to extend these ideas to truly high-dimensioned systems.

Parameterization of the Controlled System's Eigenvalues and Eigenvectors

CONSIDER a linear structure (modeled by a finite element or similar discretization scheme) in which the configuration vector x is governed by the system of differential equations

$$M\ddot{x}+C\dot{x}+Kx=Bu \tag{1}$$

where

$M=n\times n$ symmetric positive definite mass matrix
$C=n\times n$ symmetric positive semidefinite structural damping matrix
$K=n\times n$ symmetric positive semidefinite stiffness matrix
$B=n\times m$ control influence matrix
$x=n\times 1$ configuration vector
$u=m\times 1$ control vector $(\cdot)=\mathrm{d}/\mathrm{d}t(\ )$

Considering the case of linear output feedback control, let the local position, velocity, and acceleration measurements be denoted by

$$y_1=H_1x,\quad y_2=H_2\dot{x},\quad y_3=H_3\ddot{x} \tag{2}$$

which represent the linear relationship of the locally measured position y_1, velocity y_2, and acceleration y_3, where

$y_1=m_1\times$ vector $\quad H_1=m_1\times n$ matrix

$y_2=m_2\times 1$ vector $\quad H_2=m_2\times n$ matrix

$y_3=m_3\times 1$ vector $\quad H_3=m_3\times n$ matrix

For linear output feedback, we seek the constant gain matrices G_1, G_2, and G_3 so that

$$\begin{aligned}u&=-[G_1y_1+G_2y_2+G_3y_3]\\&=-G_1H_1x-G_2H_2\dot{x}-G_3H_3\ddot{x}\end{aligned} \tag{3}$$

Substitution of Eq. (3) into Eq. (1) gives the closed-loop system

$$\tilde{M}\ddot{x}+\tilde{C}\dot{x}+\tilde{K}x=0 \tag{4}$$

where the closed-loop system's matrices are

$$\tilde{M}=M+BG_3H_3,\quad \tilde{C}=C+BG_2H_2,\quad \tilde{K}=K+BG_1H_1 \tag{5}$$

Introduce the notations

$$\begin{aligned}&M=M(a), &&C=C(a), &&K=K(a)\\&B=B(c), &&H_i=H_i(b), &&G_i=G_i(g)\end{aligned} \tag{6}$$

where a is a vector of the structural and geometric model parameters (defining mass, stiffness, damping, configuration lengths, cross-sectional areas, etc.), b a vector of the sensor-type and location parameters, c a vector of the actuator-type and location parameters, and g a vector of the control gains.

Defining the $N\times 1$ global structural and control parameter vector as

$$p^T=\{a^Tb^Tc^Tg^T\} \tag{7}$$

it is apparent from Eqs. (5-7) that

$$\tilde{M}=\tilde{M}(p),\quad \tilde{C}=\tilde{C}(p),\quad \tilde{K}=\tilde{K}(p) \tag{8}$$

The details of the parameterizations of Eqs. (8) are dependent upon the particular modeling approach. Often, these are simple algebraic expressions (the elements of p appear explicitly in $\tilde{M}$, $\tilde{C}$, $\tilde{K}$).

Considering the first-order state-space differential equation, which is the equivalent to the second-order closed-loop

Received Dec. 10, 1984; revision received March 1, 1985.

*Graduate Research Assistant, Department of Engineering Science and Mechanics.
†Professor, Aerospace Engineering Department. Associate Fellow AIAA.

system of Eq. (4),

$$A\dot{z}=Bz \tag{9}$$

where

$$z=\begin{Bmatrix} x \\ \dot{x} \end{Bmatrix},\quad A=\begin{bmatrix} M & 0 \\ 0 & \tilde{M} \end{bmatrix},\quad B=\begin{bmatrix} 0 & M \\ -\tilde{K} & -\tilde{C} \end{bmatrix} \tag{10}$$

it is evident that

$$A=A(p), \qquad B=B(p), \tag{11}$$

The right and left eigenvalue problems [associated with the $z=\phi e^{\lambda t}$ solutions of Eq. (9)] are

$$\text{right: } \lambda_i A\phi_i=B\phi_i, \quad \text{left: } \lambda_i A^T\psi_i=B^T\psi_i \qquad i=1,2,\ldots,2n \tag{12}$$

where the conventional normalizations for the eigenvectors are adopted as

$$\psi_j^T A\phi_i=\delta_{ij}, \qquad \psi_j^T B\phi_i=\delta_{ij}\lambda_i \tag{13}$$

Since $A=A(p)$ and $B=B(p)$, it seems natural to consider the eigenvalues $\{\lambda_1,\ldots,\lambda_{2n}\}$ and eigenvectors $\{\phi_1,\psi_1,\ldots,\phi_{2n},\psi_{2n}\}$ to be functions of the parameter vector p, viz.,

$$\lambda_i=\lambda_i(p), \quad \phi_i=\phi_i(p), \quad \psi_i=\psi_i(p) \tag{14}$$

Except for occasional singular events (e.g., multiple eigenvalues or near-multiple eigenvalues), the nonlinear functional dependence of Eqs. (14) can be assumed to be continuous.

Qualitative Approach to Eigenspace Optimization

Most structural and control optimality criteria can be stated explicitly in terms of λ_i and ϕ_i or directly as functions of p. It is obvious that an algorithm that can effectively optimize p (over some admissible set to minimize some optimality criteria and satisfy the constraints stated as functions of p and λ_i) provides a *direct* method for controller/structure optimization problems. Unfortunately, there are several formidable difficulties, the two most prominent being:

1)The $N\times 1$ p vector is of high dimension, even for structural and control system models of moderate complexity. The dimension N of p can be several hundred.

2) The functional relationship implied by Eq. (14) is the solution fo the large eigenvalue problem of Eqs. (12) and (13). It is typically a highly nonlinear function of p and is occasionally characterized by singular local behavior (bifurcation points at repeated roots, for example).

Practical optimization algorithms that can deal with these two sources of difficulty in a rigorous and globally convergent way do not exist. However, we have developed a strategy for carrying out optimizations and suboptimizations, in spite of these two sources of difficulty. There are two heuristic ideas underlying our approach:

1) Regions of extremely high sensitivity (to the p vector) are generally undesirable. Therefore, if the performance index or constraints include a measure of eigenvalue solution sensitivity, successful suboptimizations are obviously less likely to encounter the singular events.[2]

2) Exact eigenvalue placement (or "pole placement"), for a high-order system, is not a reasonable design approach. Rather than attempting to prescribe an exact point location for every eigenvalue, it is more reasonable (and leads to better algorithms) to move all of the eigenvalues into an *acceptable region* of the complex plane. From the viewpoint of pole placement, this allows attention to be locally concentrated upon just the "problem children" eigenvalues that are the farthest outside the acceptable region or those that locally dominate a measure of optimality or sensitivity. This allows judicious and lower-dimensional suboptimizations to be made and is a key to attacking truly high-order systems.

These two qualitative ideas serve as the main motivation of our approach. Of course, an initial design point (values for the elements of p) is required. Typically, the initial design point will be the output of some (arbitrary) structural design process and, probably, a constant-gain optimal regulator design for the given structure. Thus, the present family of algorithms are designed to *begin* with the typical output of a conventional *sequential* structure—controller design process. However, for moderate-dimensional applications, we have been able to initiate control gain optimizations with a free-vibration (zero control gains) case and still achieve reliable convergence.

Central to the application of the optimization algorithms developed below lies the necessity to compute efficiently the partial derivatives of the generalized eigenvalues and eigenvectors of Eqs. (12-14). Attractive algebraic equations have been derived that explicitly determine these derivatives as "side calculations" at much less computational expense than the solution of the eigenvalue problem itself. The development of these equations is briefly summarized below for the first and second partial derivatives of the eigenvalues.

Partial Derivatives of the Closed-Loop Eigenvalues with Respect to Structural Model and Control System Parameters

Differentiating Eqs. (12) with respect to a typical element p_ℓ of p, upon premultiplying the resulting two equations by ψ_j^T and ϕ_j^T and making use of Eqs. (13), gives

$$\frac{\partial\lambda_i}{\partial p_\ell}\delta_{ij}+(\lambda_i-\lambda_j)\psi_j^T A\frac{\partial\phi_i}{\partial p_\ell}=\psi_j^T\left[\frac{\partial B}{\partial p_\ell}-\lambda_i\frac{\partial A}{\partial p_\ell}\right]\phi_i \tag{15}$$

$$\frac{\partial\lambda_i}{\partial p_\ell}\delta_{ij}+(\lambda_i-\lambda_j)\phi_j^T A^T\frac{\partial\psi_i}{\partial p_\ell}=\phi_j^T\left[\frac{\partial B^T}{\partial p_\ell}-\lambda_i\frac{\partial A^T}{\partial p_\ell}\right]\psi_i \tag{16}$$

Equations (15) and (16) hold for $i=1,2,\ldots,2n$; $j=1,2,\ldots,2n$; and $\ell=1,2,\ldots,N$. For $i=j$, both Eqs. (15) and (16) reduce to the following well-known result[1] for the gradients of the $2n$ eigenvalues

$$\frac{\partial\lambda_i}{\partial p_\ell}=\psi_i^T\left[\frac{\partial B}{\partial p_\ell}-\lambda_i\frac{\partial A}{\partial p_\ell}\right]\phi_i \tag{17}$$

Thus, having solved for eigenvalues and eigenvectors, a moderate side calculation produces the first-order eigenvalue sensitivities. Differentiating Eq. (17), with respect to p_m, we obtain the following equation for the second partial derivatives:

$$\frac{\partial^2\lambda_i}{\partial p_\ell\partial p_m}=\psi_i^T\left[\frac{\partial^2 B}{\partial p_\ell\partial p_m}-\frac{\partial\lambda_i}{\partial p_m}\frac{\partial A}{\partial p_\ell}-\lambda_i\frac{\partial^2 A}{\partial p_\ell\partial p_m}\right]\phi_i$$
$$+\frac{\partial\psi_i^T}{\partial p_m}\left[\frac{\partial B}{\partial p_\ell}-\lambda_i\frac{\partial A}{\partial p_\ell}\right]\phi_i+\psi_i^T\left[\frac{\partial B}{\partial p_\ell}-\lambda_i\frac{\partial A}{\partial p_\ell}\right]\frac{\partial\phi_i}{\partial p_m} \tag{18}$$

Since Eq. (18) involves $\partial\phi_i/\partial p_m$ and $\partial\psi_i/\partial p_m$, we must either evaluate or eliminate them. We choose the latter method. Following Plaut,[1] we project $\partial\psi_i/\partial p_m$ and $\partial\phi_i/\partial p_m$ onto the eigenvectors themselves as

$$\frac{\partial\phi_i}{\partial p_\ell}=\sum_{k=1}^{2n}a_{ki}\phi_k, \qquad \frac{\partial\psi_i}{\partial p_\ell}=\sum_{k=1}^{2n}b_{ki}\psi_k \tag{19}$$

where a_{ki} and b_{ki} are scalar constants. For $i \neq j$, substituting Eqs. (19) into Eqs. (15) and (16) yields

$$(\lambda_i - \lambda_j) a_{ji} = \psi_j^T \left[\frac{\partial B}{\partial p_\ell} - \lambda_i \frac{\partial A}{\partial p_\ell} \right] \phi_i \tag{20}$$

$$(\lambda_i - \lambda_j) b_{ji} = \phi_j^T \left[\frac{\partial B^T}{\partial p_\ell} - \lambda_i \frac{\partial A^T}{\partial p_\ell} \right] \psi_i \tag{21}$$

For the case of distinct eigenvalues, Eqs. (20) and (21) provide the a_{ji} and b_{ji} values, except for a_{ii} and b_{ii} (which remain undetermined). The normalization of Eq. (13), upon setting $j=i$ and differentiating with respect to p_ℓ and substituting Eq. (19), yields

$$a_{ii} + b_{ii} = -\psi_i^T \frac{\partial A}{\partial p_\ell} \phi_i \tag{22}$$

Substitution of Eq. (17) into Eq. (18) gives

$$\frac{\partial^2 \lambda_i}{\partial p_\ell \partial p_m} = \psi_i^T \left[\frac{\partial^2 B}{\partial p_\ell \partial p_m} - \lambda_i \frac{\partial^2 A}{\partial p_\ell \partial p_m} \right] \phi_i$$

$$- \psi_i^T G_{im} \phi_i \psi_i^T \frac{\partial A}{\partial p_\ell} \phi_i + \left\{ \frac{\partial \psi_i}{\partial p_m} \right\}^T G_{i\ell} \phi_i + \psi_i^T G_{i\ell} \frac{\partial \phi_i}{\partial p_m} \tag{23}$$

with $G_{ik} \equiv \partial B / \partial p_k - \lambda_i (\partial A / \partial p_k)$. Substitution of Eqs. (19) into Eq. (23) gives

$$\frac{\partial^2 \lambda_i}{\partial p_\ell \partial p_m} = \psi_i^T \left[\frac{\partial^2 B}{\partial p_\ell \partial p_m} - \lambda_i \frac{\partial^2 A}{\partial p_\ell \partial p_m} \right] \phi_i - \psi_i G_{im} \phi_i^T \frac{\partial A}{\partial p_\ell} \phi_i$$

$$+ (a_{ii} + b_{ii}) \psi_i^T G_{i\ell} \phi_i + \sum_{k=1, k \neq i}^{2n} [b_{ki} \psi_k^T G_{i\ell} \phi_i \quad + a_{ki} \psi_i^T G_{i\ell} \phi_k] \tag{24}$$

Finally, eliminating $a_{ii} + b_{ii}$ using Eq. (22) and a_{ji} and b_{ji} for $j \neq i$ using Eqs. (20) and (21) gives the final expressions for the second partial derivatives,

$$\frac{\partial^2 \lambda_i}{\partial p_\ell \partial p_m} = \psi_i^T \left[\frac{\partial^2 B}{\partial p_\ell \partial p_m} - \lambda_i \frac{\partial^2 A}{\partial p_\ell \partial p_m} \right] \phi_i$$

$$- \psi_i^T G_{im} \phi_i \psi_i^T \frac{\partial A}{\partial p_\ell} \phi_i - \psi_i^T \frac{\partial A}{\partial p_m} \phi_i \psi_i^T G_{i\ell} \phi$$

$$+ \sum_{k=1, k \neq i}^{2n} \left[\frac{\psi_i^T G_{im} \phi_k \psi_k^T G_{i\ell} \phi_i + \psi_k^T G_{im} \phi_i \psi_i^T G_{i\ell} \phi_k}{(\lambda_i - \lambda_k)} \right] \tag{25}$$

which, of course, are singular for repeated eigenvalues.

Closed-Loop Response

The response of the controlled configuation to initial disturbances is determined using a modal approach. The modal coordinates η are mapped into the state space by

$$z = [\phi] \eta, \qquad \dot{z} = [\phi] \dot{\eta} \tag{26}$$

where $[\phi]$ is the right modal matrix. Substituting Eqs. (26) into Eq. (9), premultiplying by $[\psi]^T$ (the left modal matrix) and utilizing Eqs. (13), the equations of motion are uncoupled and given by

$$\dot{\eta}_i = \lambda_i \eta_i, \qquad i = 1,2,\ldots,2n \tag{27}$$

The solution to Eq. (27) is

$$\eta_i = e^{\lambda_i (t - t_0)} \eta_i(t_0), \qquad i = 1,2,\ldots 2n \tag{28}$$

The initial conditions are mapped into modal space by premultiplying Eqs. (26) by $[\phi]^{-1} = [\psi]^T A$ and utilizing Eq. (13) to give

$$\eta(t_0) = [\psi]^T A z(t_0) \tag{29}$$

The system response in normal coordinates is then given by Eqs. (28) and (29). However, the eigenvalues and eigenvectors are in the general complex consisting of n eigenvalues and n eigenvectors plus their associated n complex conjugates. We seek a solution that will eliminate the complex conjugates and thus allow us to truncate the number of modes used in the solution.

The modal matrices are partitioned as follows:

$$[\psi] = \begin{bmatrix} \psi_1 & \bar{\psi}_1 \\ \psi_2 & \bar{\psi}_2 \end{bmatrix}, \quad [\phi] = \begin{bmatrix} \phi_1 & \bar{\phi}_1 \\ \phi_2 & \bar{\phi}_2 \end{bmatrix} \tag{30}$$

where ψ_1, ψ_2, ϕ_1, and ϕ_2 are $n \times k$ matrices normalized by Eqs. (13). It follows that $\bar{\psi}_1$, $\bar{\psi}_2$, $\bar{\phi}_1$, and $\bar{\phi}_2$ are also $n \times k$ matrices and are thus the complex conjugates of ψ_1, ψ_2, ϕ_2, respectively. The vector of normal coordinates η can also be partitioned as

$$\eta = \begin{Bmatrix} \zeta \\ \bar{\zeta} \end{Bmatrix} \tag{31}$$

where ζ is a $k \times 1$ vector. It can be shown that $\bar{\zeta}$ is also $k \times 1$ and is the complex conjugate of ζ. Substituting Eqs. (30) and (31) into Eq. (26), the response in configuration coordinates is

$$z = \begin{Bmatrix} x \\ \dot{x} \end{Bmatrix} = \begin{Bmatrix} \phi_1 \zeta + \bar{\phi}_1 \bar{\zeta} \\ \phi_2 \zeta + \bar{\phi}_2 \bar{\zeta} \end{Bmatrix}$$

$$= 2 \begin{Bmatrix} [Re\phi_1]\{Re\zeta\} - [Im\phi_1]\{Im\zeta\} \\ [Re\phi_2]\{Re\zeta\} - [Im\phi_2]\{Im\zeta\} \end{Bmatrix} \tag{32}$$

From Eq. (32), it is evident that the complex conjugates of the n eigenvalues and eigenvectors are not needed and that the k modes can be used to determine the response. The measured beam deflections and deflection rates follow from Eq. (2) and the controlled response from Eq. (3).

A Model of Draper/RPL Configuration

Referring to Figs. 1 and 2, we consider the planar rotational/vibrational dynamics of the demonstration experimental model sponsored by the U.S. Air Force Rocket Propulsion Laboratory for testing the control laws for maneuvering flexible spacecraft; this experimental work is presently being conducted at the C.S. Draper Laboratory.[2] The central hub is supported by an air bearing table with four appendages cantilevered from the hub. Table 1 summarizes the Draper/RPL configuration parameters. Following Turner and Chun,[2] we form a discretized model for the system by assuming that the elastic deformations of each of the arms (relative to a body-fixed undeformed state) can be represented as linear combination of the comparison functions.

$$\phi_k(z) = 1 - \cos\left(\frac{k\pi z}{L}\right) + \frac{1}{2}(-1)^{k+1}\left(\frac{k\pi z}{L}\right)^2 \tag{33}$$

so that the transverse body-fixed deformation of the jth arm is modeled as

$$y_j(t,z) = \sum_{k=1}^{\tilde{N}} q_{kj}(t) \phi_k(z), \qquad j = 1,2,3,4, \quad 0 \leq z \leq L \tag{34}$$

Radial elongation of the arms is neglected, as are out-of-plane deformations. For the numerical results presented below, we took $\bar{N}=10$. Using Eq. (34) to evaluate the potential and kinetic energy[3] leads to equations of the form of Eq. (1), with the configuration vector

$$x=[\theta\,\vdots\,q_{11}q_{21}\cdots\,\vdots\,q_{\bar{N}1}\,\vdots\,q_{12}q_{22}\cdots q_{\bar{N}2}\,\vdots\cdots q_{14}q_{24}\cdots q_{\bar{N}4}]^T$$

We restrict attention to the class of antisymmetric deformations whereby $y_1(t,z)\equiv y_2(t,z)$ and $y_3(t,z)\equiv y_4(t,z)$; thus, $q_{il}(t)\equiv q_{i2}(t)$ and $q_{i3}(t)\equiv q_{i4}(t)$. For this class of antisymmetric motions, the configuration vector can be collapsed to

$$x=[\theta\,\vdots\,q_{11}q_{21}\cdots q_{\bar{N}1}\,\vdots\,q_{13}q_{23}\cdots q_{\bar{N}3}]^T \tag{35}$$

For $\bar{N}=10$, the order of the system of Eq. (1) is thus 21. The explicit expressions for the elements of the M and K matrices are developed in Ref. 3. We take $C=\mu K$, where μ is a constant. For the numerical examples presented, $\mu=1\cdot E-5$; the controlled response of the first seven modes is insensitive to an order of magnitude variation of μ. In Fig. 3, we show the first nine normal modes.

The eigenvalues and eigenvectors for the first seven modes have converged in the numerical sense that increasing $\bar{N}$ does not change the first four or five digits, whereas modes eight and nine have converged to about three digits. (However, the last ten higher-frequency computed eigenvalues and eigenvectors, as expected, are not as accurately calculated.) Thus, we restrict our optimization discussions to the first nine modes. After the first (rigid-body) mode, the remaining modes occur in near pairs. The antisymmetic, "opposition" modes are simple cantilever beam modes characterized by the adjacent beams moving in opposition (the constraint torques between the hub and the beam clamp cancel in equal and opposite pairs, resulting in a zero rotation of the hub). The antisymmetric "unison" modes are perturbed cantilever modes (with varied frequencies) characterized by all four beams moving in unison; the hub has nonzero rotation for these modes. As is evident, the corresponding pair of unison and opposition frequencies are closely spaced; this spacing decreases with increasing mode number.

Table 1 Draper/RPL configuration parameters

Hub radius	1ft
Rotary inertia of hub, r	8 slug-ft^2
Mass density of beams, ρ	5.22 slug/ft^3
Elastic modulus of the arms, E	1.1×10^7 lb/in.^{2}
Arm thickness, t_a	0.125 in.
Arm height, h_a	6 in.
Arm length, L	4 ft
Tip mass	0.156941 slug
Rotary inertia of tip masses	0.0018 slug-ft^2

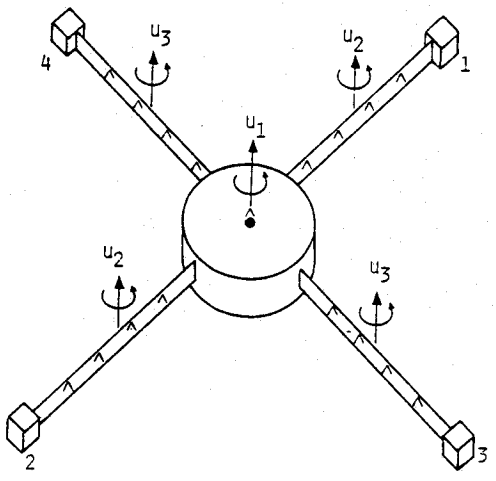

Fig. 1 The Draper/RPL configuration.

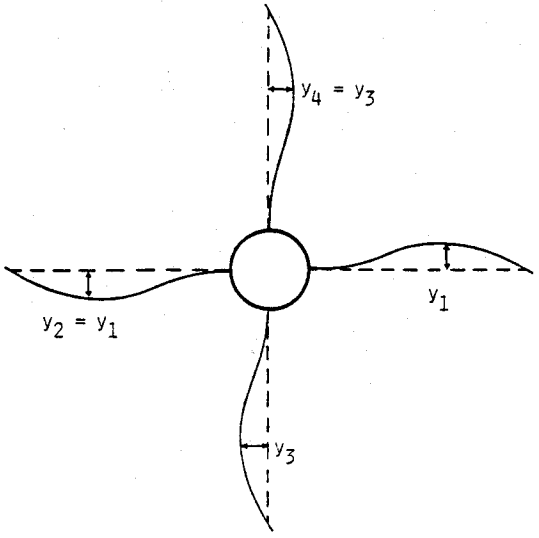

Fig. 2 Anti-symmetric deformation.

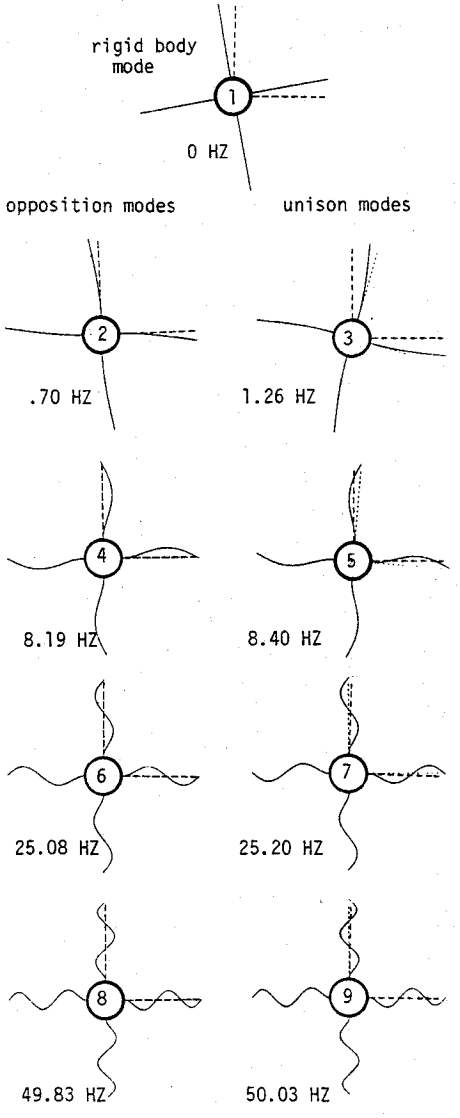

Fig. 3 First nine normal modes.

Actuator/Sensor Configuration

We admit torque actuators on the central hub and at some station z on each appendage. We also admit rotational position and velocity sensors on the hub and deflection and deflection rate sensors at some stations on each appendage. For the case in which the actuators consist of a torque u_1 applied to the hub, a torque u_2 applied at station z_1 on appendages 1 and 2, and a torque u_3 applied at station z_2 on appendages 3 and 4, the right-hand side of Eq. (1) is

$$Bu = \begin{bmatrix} 1 & 2 & 2 \\ 0 & 2\phi'(z_1) & 0 \\ 0 & 0 & 2\phi'(z_2) \end{bmatrix} \begin{Bmatrix} u_1 \\ u_2 \\ u_3 \end{Bmatrix} \tag{36}$$

where

$$\phi'(z) = \frac{d}{dz}[\phi(z)], \quad \phi(z) = [\phi_1(z) \ldots \phi_{10}(z)]^T$$

and, if rotational position and velocity sensors are located on the hub, while colocated deflectional position and velocity sensors are located at stations $x_1,\ldots,x_8$ on each appendage then the sensor influence matrices H_1, H_2 are both the same 9×21 matrix,

$$H_i = \begin{bmatrix} 1 & 0^T & 0^T \\ 0 & \phi^T(x_1) & 0^T \\ \vdots & \vdots & \vdots \\ 0 & \phi^T(x_4) & 0^T \\ 0 & 0^T & \phi^T(x_5) \\ \vdots & \vdots & \vdots \\ 0 & 0^T & \phi^T(x_8) \end{bmatrix}, \quad i=1,2 \tag{37}$$

and

$$y_1^T = [\theta y_1(t,x_1) \ldots y_1(t,x_4) y_3(t,x_5) \ldots y_3(t,x_8)], \quad y_2 = \frac{d}{dt}(y_1) \tag{38}$$

and the gains G_1 and G_2 are both 3×9 matrcies. For the numerical examples below, we initially set $z_1 = z_2 = L/2$, $x_1 = x_5 = L/4$, $x_2 = x_6 = L/2$, $x_3 = x_7 = 0.7L$, $x_4 = x_8 = 0.9L$, and selectively admit structural parameters, actuator locations, and sensor locations along with the control gain vector in p.

Minimum Modification Strategy for Structural/Controller Design Iterations

Consider a constrained optimization problem wherein we seek the optimal value of the parameter vector p that extremizes some performance measure

$$J = J[\lambda_1(p),\ldots,\lambda_{2n}(p), \quad \phi_1(p),\ldots,\phi_2(p),p] \tag{39}$$

subject to the satisfaction of the N_α equality constraints

$$\alpha_j[\lambda_1(p),\ldots,\lambda_{2n}(p), \quad \phi_1(p),\ldots,\phi_{2n}(p),p] = 0$$
$$j = 1,2,\ldots,N_\alpha \tag{40}$$

and N_β inequality constraints

$$\beta_{jL} \le \beta_j[\lambda_1(p)\ldots,\lambda_{2n}(p), \quad \phi_1(p)\ldots,\phi_{2n}(p),p] \le \beta_{jU}$$
$$j = 1,2,\ldots,N_\beta \tag{41}$$

Thus, the performance measure and constraints are defined in terms of the eigensolution, but we also admit explicit dependence upon p to include, for example, structure and control system criteria. Equations (39-41) define a nonlinear programming problem for which a number of algorithms have been developed and applied during the past two decades.[4-6] One iteration stategy confines local attention to only the locally violated inequality constraints and all of the functions of Eqs. (39) and (40). Specifically, one can seek the smallest correction vector Δp that achieves specified increments of ΔJ, $\Delta\alpha_j$, and $\Delta\beta_j$ for a subset of the functions of Eqs. (39-41). Linearizing these equations about p_i results in

$$\Delta\gamma = \left[\frac{\partial\gamma}{\partial p}\bigg|_{p_i}\right]\Delta p \tag{42}$$

where $\gamma = [J,\alpha_j,\beta_j]^T$. Since Eqs. (42) constitute, typically, a small number of equations in a large number of unknowns, we expect an infinity of exact Δp solutions; some criterion must be introduced to select a particular solution. Motivated by the desire to satisfy, as nearly as possible, the implicit local linearity assumption, we seek a "small Δp" solution. Minimizing the correction norm $\Delta p^T W \Delta p$ (for W a suitable weight matrix) subject to Eq. (42) gives

$$\Delta p = W^{-1}\left[\frac{\partial\gamma}{\partial p}\bigg|_{p_i}\right]^T \Lambda \tag{43a}$$

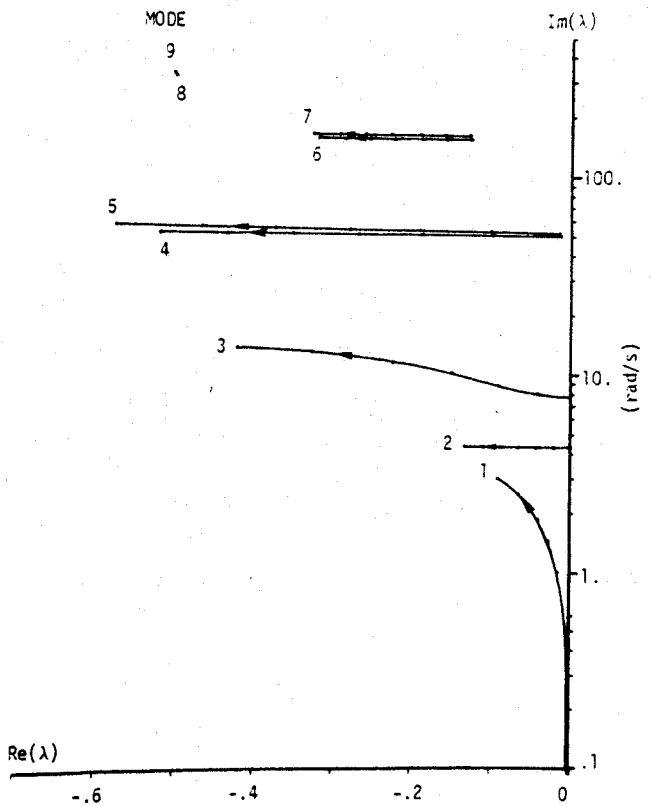

Fig. 4 Eigenvalue placement locus of first nine modes: case 1 (continuation parameter α varys from zero to one in six increments from right to left along each eigenvalue trajectory).

where Λ is a Lagrange multiplier vector obtained by solving

$$\left[\frac{\partial\gamma}{\partial p}\bigg|_{p_i}\right] W^{-1}\left[\frac{\partial\gamma}{\partial p}\bigg|_{p_i}\right]^T \Lambda = \Delta\gamma \tag{43b}$$

Thus, the size of the linear system we must solve is equal to the number of functions [from Eqs. (39-41)] that we seek to change by the increment vector $\Delta\gamma$, regardless of the number of elements in the Δp vector. The partial derivatives needed in Eq. (42) can be evaluated by the chain rule partial differentiation of Eqs. (38-40), making use of the eigenvalue gradients of Eq. (17). Of course, second-order optimization algorithms can also be used,[5] in which case one will need the second partial derivatives of Eqs. (25).

As a nonlinear programming strategy, we first seek a nearest *feasible* p, which satisfies all of the constraints [Eqs. (40) and (41)] and then include J increments in $\Delta\gamma$ to seek a constrained optimal solution. This strategy can be formalized[4]; it is fully equivalent to the gradient projection constrained optimization algorithms.

For example, we can apply the above developments to place the Draper/RPL system's closed-loop eigenvalues in a desired region and, subject to this condition, minimize a robustness measure (e.g., the sensitivity of the eigenvalues with respect to variation of uncertain system parameters).

Numerical Examples: Eigenvalue Placement for the Draper/RPL Configuration

Case 1

This first example is a modification of a result presented in Ref. 2. We consider the problem of finding a minimum norm gain vector $g \equiv p$ (42 elements of G_1 and G_2) that results in the eigenvalues of the closed-loop system [Eq. (9)] satisfying the prescribed constraints of

$$\gamma_{\text{objective}} - \gamma(g) = 0 \tag{44}$$

where, in particular, we consider the constraint vector

$$\gamma(g) = [\omega_1(g)\ \zeta_1(g)\ \zeta_2(g) \ldots \zeta_9(g)]^T \tag{45}$$

The damping factors $\zeta_i(g)$ and damped frequencies $\omega_i(g)$ are related to the eigenvalues $\lambda_i(g)$ as

$$\zeta_i = -Re[\lambda_i(g)] / \{[(Re\lambda_i(g)]^2 + [Im\lambda_i(g)]^2\}^{1/2}$$

$$\omega_i = Im[\lambda_i(g)], \qquad i = 1,2,\ldots \tag{46}$$

The eigenvalues are labeled according to the ordering

$$|Im\lambda_1(g)| \le |Im\lambda_2(g)| \le \ldots \le |Im\lambda_i(g)| \tag{47}$$

The objective values of the damping factors and the first natural frequency (the elements of $\gamma_{\text{objective}}$), for the specific numerical example here, are prescribed as

$$\gamma_{\text{objective}} = [3.0\ 0.03\ 0.03\ 0.03\ 0.01\ 0.01\ 0.002\ 0.002\ 0.0015\ 0.0015] \tag{48}$$

In order to enhance the convergence, a continuation procedure is used: Eq. (44) is replaced by the one-parameter (α) family

$$\alpha\gamma_{\text{objective}} - \gamma[g(\alpha)] = 0, \quad 0 \le \alpha \le 1 \tag{49}$$

Obviously, $\alpha = 0$ results in the trivial solution $g(0) = 0$ (corresponding to free, uncontrolled vibration), whereas $g(1)$ is the desired solution [since Eq. (49) becomes identical to Eq. (44)]. Sweeping α from 0 to 1 allows us to define "stepping-stone" problems that are arbitrarily near the converged neighboring solutions; thus, the generalized Newton algorithms using Eq. (43), with $W = I$ and $p \equiv g$, can be initiated with an arbitrarily close starting estimate and very nearly guarantee satisfaction of the implicit linearity assumption. For the particular calculations herein, we found rather large α increments of 1/6 led to reliable convergence. Thus, six intermediate α solutions were required to achieve final convergence; for each α value, two or three iterations [Eq. (43)] were required to find the $g(\alpha)$ satisfying Eq. (49).

As a specific example, we used the initial g vector (displayed as the elements of G_1 and G_2),

$$G_1 = G_2 = \begin{bmatrix} 0.001 & 0 & 0 & 0 & 0 & 0 & 0 & 0 & 0 \\ 0 & 0 & 0 & 0 & 0 & 0 & 0 & 0 & 0 \\ 0 & 0 & 0 & 0 & 0 & 0 & 0 & 0 & 0 \end{bmatrix}$$

The (1,1) elements were set slightly nonzero, since exactly zero causes the "rigid-body" eigenvalue to be zero with a resulting

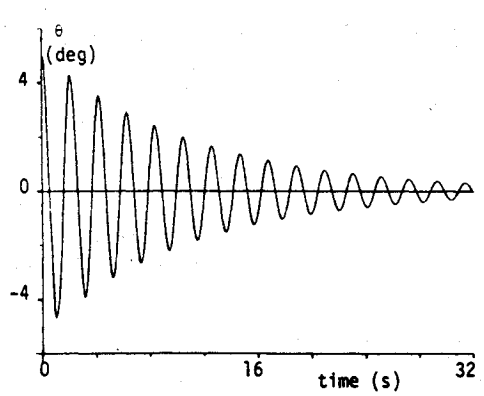

Fig. 5 Closed-loop response of $\theta(t)$: case 1.

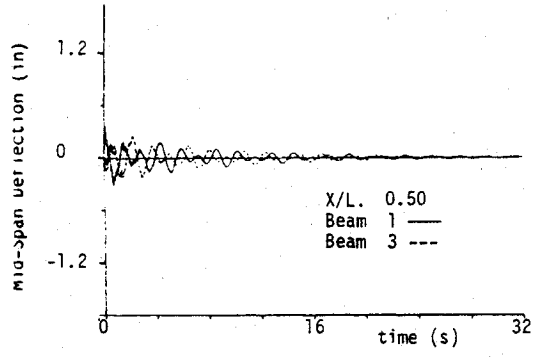

Fig. 6 Beam deflection response (midspan stations): case 1.

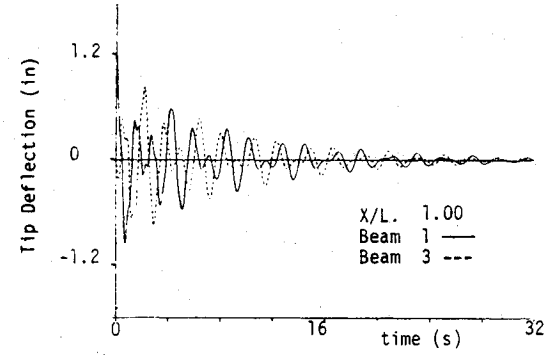

Fig. 7 Beam deflection response (tip stations): case 1.

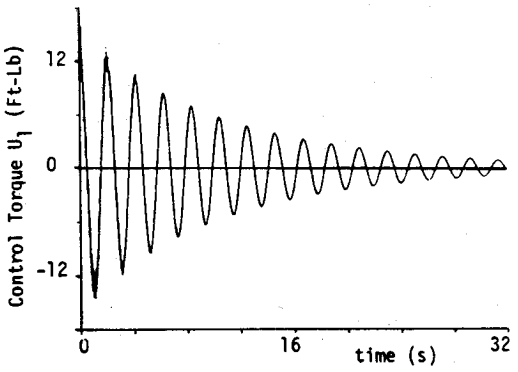

Fig. 8 Control torque $U_1(t)$: case 1.

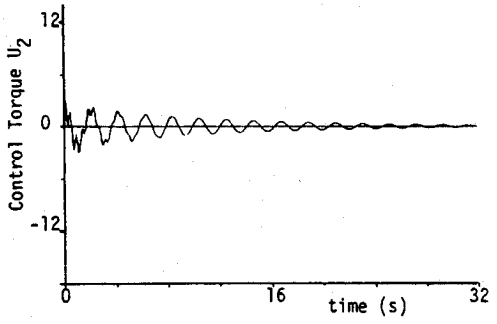

Fig. 9 Control torque $U_2(t)$: case 1.

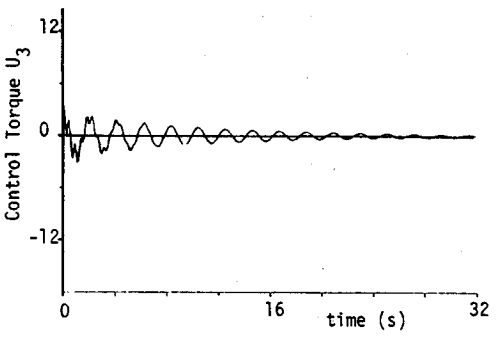

Fig. 10 Control torque $U_3(t)$: case 1.

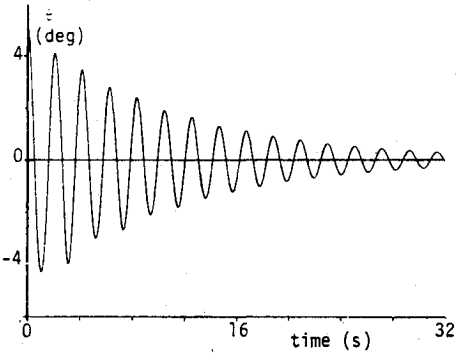

Fig. 11 Closed-loop response of $\theta(t)$: case 2.

rank-deficient linear system (because the damping ratio sensitivity vanishes if $\lambda_1 \to 0$).

The final converged gain matrices were found to be (only three digits are shown)

$$G_1 = \begin{bmatrix} 153 & 4.38 & .0 & 21.5 & .0 & 4.38 & 0.0 & 21.5 & 0.0 \\ 0.0 & 2.66 & 7.89 & 13.9 & 22.5 & 2.65 & 7.89 & 13.9 & 22.5 \\ 0.0 & 2.66 & 7.89 & 13.9 & 22.5 & 2.65 & 7.89 & 13.9 & 22.5 \end{bmatrix} \tag{50a}$$

$$G_2 = \begin{bmatrix} 4.06 & -0.389 & 0.0 & -1.73 & 0.0 & -0.389 & 0.0 & -1.73 & 0.0 \\ 0.0 & 0.094 & -0.036 & 0.188 & -0.100 & 0.061 & -0.170 & 0.135 & -0.211 \\ 0.0 & 0.061 & 0.170 & 0.135 & -0.211 & 0.094 & -0.036 & 0.188 & -0.100 \end{bmatrix} \tag{50b}$$

where the 12 zeros indicate elements of G_1 and G_2 not used in p. The locii of the first nine closed-loop eigenvalues are plotted in Fig. 4 for $0 \leq \alpha \leq 1$, with $\alpha = 0$ the point nearest the imaginary axis in all cases. Note that, for eigenvalues 8 and 9, the structural damping produced damping factors exceeding the objective damping factors and thus these eigenvalues experienced little movement. All other higher calculated eigenvalues [Eqs. (10-12)] remained in the left half-plane, although this does not occur if the structural damping is assumed negligible.

The closed-loop response for the controlled configuration was calculated for initial disturbances of $\theta(t_0) = 5$ deg rigid-body rotation and $q_{11}(t_0) = 0.02$, which corresponds to a tip deflection of 1.66 in. for arms 1 and 2. The hub angle time history and beam deflection time histories for $z/L = \frac{1}{2}$ and 1 are illustrated in Figs. 5-7, respectively. The torque actuator responses are shown in Figs. 8-10 for actuators u_1, u_2, and u_3, respectively. In Fig. 8, it can be seen that there are high-frequency oscillations superimposed on the first few cycles of the low-frequency response. This is due to the high-frequency vibration of modes 8 and 9, but these are quickly damped out due to the structural and controller damping. Also, note that u_1 is doing most of the work compared to u_2 and u_3, a desired result, even though we have not forced this condition by weighting.

Case 2

This case is the same as case 1 except that we modified the parameter vector to include the sensor and actuator locations, in addition to the 42 control gains of case 1, as

$$\begin{aligned} p &= \text{actuator location vector } c \\ &= \text{sensor location vector } b \\ &= \text{gain vector } g \end{aligned} \tag{51}$$

Thus, the two appendage actuator stations (z_1, z_2) plus the eight actuator sensor $(x_1, \ldots, x_8)$ stations brings the total dimension of p to 52. Upon applying the minimum norm correction of Eq. (43) to satisfy the constraint of Eq. (44), with $W = I$, we found the sensor and actuator stations were moving undesirably large amounts, so we introduced weights of 10^2 on the actuator positions and the two inboard sensor stations, while a weight of 10^3 was applied to the two outboard sensors. With this modest artwork on the weight selection, the minimum norm algorithm was applied (with six continuation

steps as in case 1) and reliable covergence ensued to place the eigenvalues to satisfy Eqs. (44) and (48).

The resulting converged gain matrices were found to be

$$G_1 = \begin{bmatrix} 92.1 & 1.71 & 0.0 & 10.5 & 0.0 & 1.75 & 0.0 & 10.7 & 0.0 \\ 0.0 & 1.55 & 4.93 & 9.36 & 15.2 & 1.57 & 5.06 & 9.56 & 15.5 \\ 0.0 & 1.57 & 4.85 & 9.15 & 14.9 & 1.59 & 4.98 & 9.38 & 15.2 \end{bmatrix} \tag{52a}$$

$$G_2 = \begin{bmatrix} -4.14 & -0.165 & 0.0 & -2.43 & 0.0 & -0.305 & 0.0 & -2.80 & 0.0 \\ 0.0 & -1.09 & 2.07 & -2.80 & 4.54 & -1.13 & 1.43 & -2.76 & 3.87 \\ 0.0 & -1.10 & 1.85 & -2.60 & 4.28 & -1.21 & 1.72 & -3.04 & 4.46 \end{bmatrix} \tag{52b}$$

and the converged (initial values in parenthesis) appendage actuator stations were

$$z_1 = 0.1959\,L \ (0.5\,L), \text{ on appendages 1 and 2}$$

$$z_2 = 0.1841\,L \ (0.5\,L), \text{ on appendages 3 and 4} \tag{53}$$

whereas the converged (initial) sensor stations were, on appendages 1 and 2,

$$x_1 = 0.2546 \ (0.25\,L) \qquad x_3 = 0.7155 \ (0.7\,L)$$

$$x_2 = 0.5414 \ (0.5\,L) \qquad x_4 = 0.9317 \ (0.9\,L) \tag{54a}$$

and on appendages 3 and 4,

$$x_5 = 0.2564 \ (0.25\,L)$$

$$x_6 = 0.5443 \ (0.5\,L)$$

$$x_7 = 0.7167 \ (0.7\,L)$$

$$x_8 = 0.9321 \ (0.9\,L) \tag{54b}$$

The continuation/root locus of the eigenvalues is essentially identical to Fig. 4. However, the freedom to move the sensor and actuator locations has proved constructive; by comparison of Eqs. (50) and (52), it is obvious that the gains have been substantially reduced. Note in Eq. (53) that the appendage torquers hae been moved much closer to the hub, whereas the sensors have been moded significantly away from the hub. The net effect is that, even though the closed-loop eigenvalues have the same position, smaller control torques are required. This is evident in comparing the controlled response of case 2 to the same initial conditions as case 1 (Figs. 11-16), with the corresponding figures of case 1 (Figs. 5-10). Note that the peak torque is 17 ft-lb for case 1, whereas it is only 13 ft-lb for case 2. The controlled response is virtually unchanged (as might be expected, since the two sets of eigenvalues are the same).

Case 3

This case is the same as case 2 with two new ingredients: 1) two structural parameters the appendage length L and the tip mass m_{tip} are varied to provide some structural design control over the free-vibration frequency spectrum of the structure; and 2) in comparison to case 2, the case 3 controlled "rigid-body mode" eigenvalue is constrained to be the lower

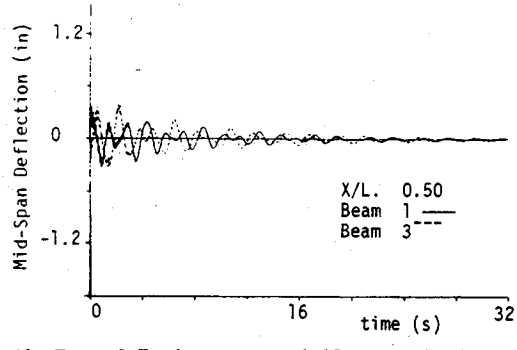

Fig. 12 Beam deflection response (midspan stations): case 2.

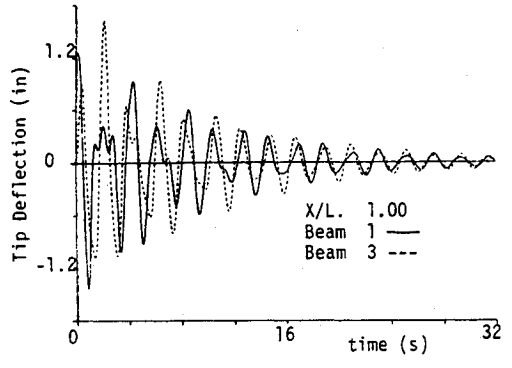

Fig. 13 Beam deflection response (tip stations): case 2.

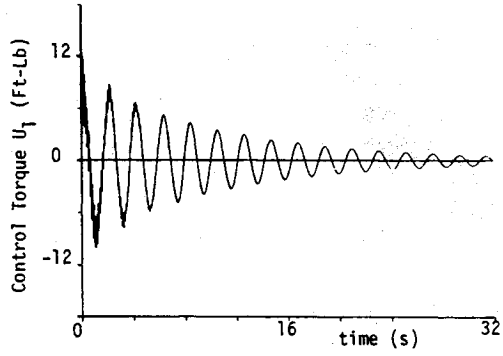

Fig. 14 Control torque $U_1(t)$: case 2.

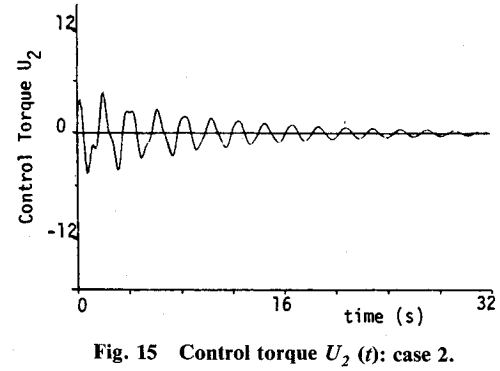

Fig. 15 Control torque U_2 (t): case 2.

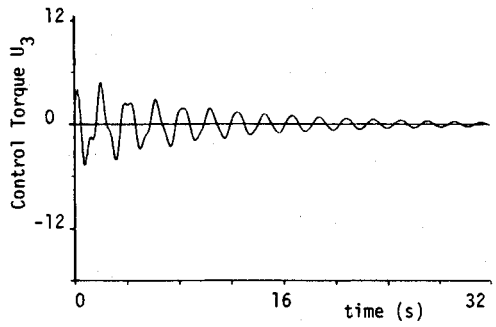

Fig. 16 Control torque $U_3(t)$: case 2.

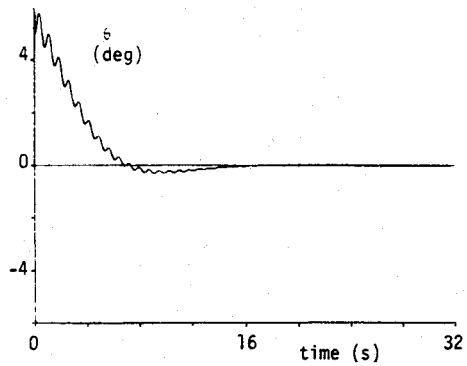

Fig. 17 Closed-loop response of $\theta(t)$: case 3.

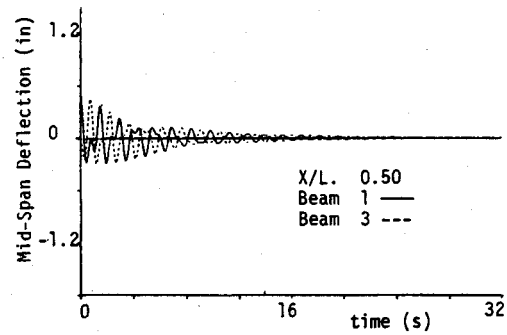

Fig. 18 Beam deflection response (midspan stations): case 3.

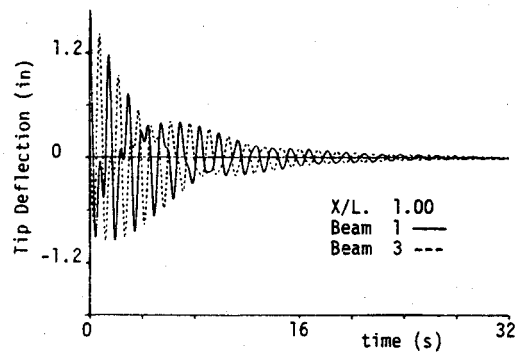

Fig. 19 Beam deflection response (tip stations): case 3.

frequency and is much more heavily damped, to be consistent with a "slewing" attitude maneuver/vibration arrest control law.

Thus, we adopt the following 12 objective constraints for the closed-loop eigenvalues (where the nonzero numbers in parentheses indicate initial natural frequencies of original uncontrolled configuration):

$\gamma_{\text{objective}} =$

$$\left\{\begin{array}{lll}
\omega_1 = 0.3\ r/s & (0) & \text{rigid body mode frequency} \\
\omega_2 = 4.5\ r/s & (4.37) & \text{first flexural mode frequency} \\
\omega_3 = 8.3\ r/s & (7.91) & \text{second flexural mode frequency} \\
\zeta_1 = 0.7 & (0) & \text{rigid body mode damping factor} \\
\zeta_2 = 0.03 & (0) & \text{first flexible mode damping factor} \\
\zeta_3 = 0.03 & (0) & \text{second flexible mode damping factor} \\
\zeta_4 = 0.01 & (0) & \text{third flexible mode damping factor} \\
\zeta_5 = 0.01 & (0) & \text{fourth flexible mode damping factor} \\
\zeta_6 = 0.002 & (0) & \text{fifth flexible mode damping factor} \\
\zeta_7 = 0.002 & (0) & \text{sixth flexible mode damping factor} \\
\zeta_8 = 0.0015 & (0) & \text{seventh flexible mode damping factor} \\
\zeta_9 = 0.0015 & (0) & \text{eighth flexible mode damping factor}
\end{array}\right\} \tag{55}$$

These constraints were imposed in two stages. First, the structural parameters (L, M_{tip}) were adjusted to drive ω_2 and ω_3 to their objective values. In the second stage, the 52 control gains and sensor/actuator stations are modified (in 6 continuation steps as in case 2) to drive γ to the above objective values. Convergence was reliably obtained and the resulting control were found to be

$$G_1 = \begin{bmatrix} 4.84 & 0.148 & 0.0 & 1.01 & 0.0 & 0.148 & 0.0 & 0.101 & 0.0 \\ 0.0 & 0.034 & 0.116 & 0.214 & 0.315 & 0.037 & 0.125 & 0.231 & 0.341 \\ 0.0 & 0.036 & 0.125 & 0.231 & 0.341 & 0.034 & 0.116 & 0.214 & 0.315 \end{bmatrix} \tag{56a}$$

$$G_2 = \begin{bmatrix} 16.3 & -0.026 & 0.0 & -0.148 & 0.0 & -0.026 & 0.0 & -0.148 & 0.0 \\ 0.0 & 0.065 & 0.011 & 0.138 & -0.256 & -0.066 & -0.068 & 0.111 & -0.068 \\ 0.0 & 0.066 & -0.448 & -0.111 & -0.448 & 0.065 & 0.011 & 0.137 & -0.256 \end{bmatrix} \tag{56b}$$

The converged (initial) appendage actuator positions were

$$z_1 = 0.4102\ L\ (0.5\ L), \text{ on appendages 1 and 2}$$
$$z_2 = 0.4102\ L\ (0.5\ L), \text{ on appendages 3 and 4} \tag{57}$$

whereas the converged (initial) appendage sensor positions were, on appendages 1 and 2,

$$\begin{aligned} x_1 &= 0.2539\ L\ (0.25\ L) \\ x_2 &= 0.5010\ L\ (0.5\ L) \\ x_3 &= 0.7608\ L\ (0.7\ L) \\ x_4 &= 0.9653\ L\ (0.9\ L) \end{aligned} \tag{58a}$$

and on appendages 3 and 4,

$$\begin{aligned} x_5 &= 0.2539\ L\ (0.25\ L) \\ x_6 &= 0.5010\ L\ (0.5\ L) \\ x_7 &= 0.7608\ L\ (0.7\ L) \\ x_8 &= 0.9653\ L\ (0.9\ L) \end{aligned} \tag{58b}$$

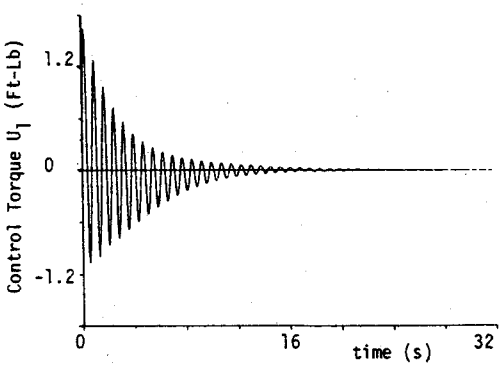

Fig. 20 Control torque $U_1(t)$: case 3.

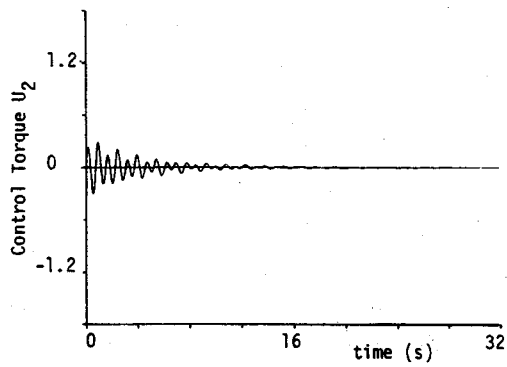

Fig. 21 Control torque $U_2(t)$: case 3.

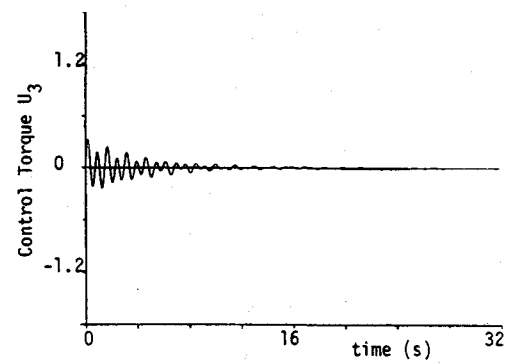

Fig. 22 Control torque $U_3(t)$: case 3.

The converged (initial) values for L and M_{tip} were found to be

$L = 3.67$ ft (4 ft)

$M_{tip} = 0.19871$ slugs (0.156941 slugs)

The controlled response for case 3 is given in Figs. 17-22 for comparison with cases 1 and 2. Note the following features: 1) the rigid-body maneuver and complete vibration arrest is accomplished in approximately 15 s (about half the time required for cases 1 and 2); 2) the peak control torque is reduced by about an order of magnitude; and 3) the location of sensors is not significantly different from case 2, but the actuator positions are different (closer to midspan). It is also evident that the present maneuver controls are much more attractive than cases 1 and 2. We have done a variety of parameter variations further establishing that the rigid-body eigenvalue placement is the most important feature of case 3. For any reasonable variation of the sensor/actuator stations and/or structural parameters, we can optimize the control gains to place the eigenvalues in the same position and achieve analogous results.

Conclusions

We have developed and demonstated a minimum modification strategy for structural and control parameter optimization. Numerical experience indicates occasional difficulties with the uncontrolled modes being destabilized, but since all of the eigenvalues (up through a conservative number) are calculated on each iteration, these problems can be circumvented by introducing appropriate constraints to stabilize these modes. The method has worked well on the problems studied to date and appears to be an attractive approach to follow in the development of an interactive software system for structure/controller design iterations. Extension of the ideas of this paper to determine the weight matrices for imposing eigenvalue placement upon optimal quadratic regulators is presented in Ref. 8. The algorithms presented herein have been found relatively immune to the high dimensionality and nonlinearity of the eigenvalue placement problem.

Acknowledgment

This work was sponsored by the Air Force Office of Scientific Research under Contract F4920-83-K-D032.

References

[1]Plaut, R.H. and Huseyin, K., "Derivatives of Eigenvalues and Eigenvectors in Non-Self-Adjoint Systems," *AIAA Journal,* Vol. 11, Feb. 1973, pp. 250-251.

[2]Turner, J.D. and Chun, H.M., "Optimal Feedback Control of a Flexible Spacecraft During a Large Angle Rotational Maneuver," AIAA Paper 82-1589, Aug. 1982.

[3]Chun, H.M., "Optimal Distributed Control of a Flexible Spacecraft During a Large Angle Rotational Maneuver," MS Thesis, Massachusetts Institute of Technology, Cambridge, June 1982.

[4]Junkins, J.L., "Equivalence of the Minimum Norm and Gradient Projection Constrained Optimization Techniques," *AIAA Journal,* Vol. 10, July 1972, pp. 927-929.

[5]Fiacco, A.V. and McCormick, G.P., *Nonlinear Programming; Sequential Unconstrained Minimization Techniques,* John Wiley & Sons, New York, 1968.

[6]Anderson, L., "Direct Design of Multivariable Control Systems Through Singular Value Decomposition," AAS/AIAA Astrodynamics Conference, Aug. 1983,

[7]Junkins, J.L., Bodden, D.S., and Kamat, M.P., "An Eigenvalue Optimization Approach for Feedback Control of Flexible Structures," presented at SECTAM XII, Calloway Gardens, GA., May 1984.

[8]Junkins, J.L. Bodden, D.S., and Turner, J.C., "A Unified Approach to Structure and Control System Design Iterations," *Proceedings of 4th International Conference on Applied Numerical Modeling,* Society of Theoretical and Applied Mechanics, Republic of China, Dec. 1984, pp. 483-490.